

Accepted Manuscript

Journal of the Geological Society

The source of topography across the Cumberland Peninsula, Baffin Island, Arctic Canada: differential exhumation of a North Atlantic rift flank

Scott Jess, Randell Stephenson, Søren B. Nielsen & Roderick Brown

DOI: <https://doi.org/10.1144/jgs2018-211>

Received 30 November 2018

Revised 23 May 2019

Accepted 27 May 2019

© 2019 The Author(s). This is an Open Access article distributed under the terms of the Creative Commons Attribution 4.0 License (<http://creativecommons.org/licenses/by/4.0/>). Published by The Geological Society of London. Publishing disclaimer: www.geolsoc.org.uk/pub_ethics

Supplementary material at <https://doi.org/10.6084/m9.figshare.c.4528409>

To cite this article, please follow the guidance at http://www.geolsoc.org.uk/onlinefirst#cit_journal

Manuscript version: Accepted Manuscript

This is a PDF of an unedited manuscript that has been accepted for publication. The manuscript will undergo copyediting, typesetting and correction before it is published in its final form. Please note that during the production process errors may be discovered which could affect the content, and all legal disclaimers that apply to the journal pertain.

Although reasonable efforts have been made to obtain all necessary permissions from third parties to include their copyrighted content within this article, their full citation and copyright line may not be present in this Accepted Manuscript version. Before using any content from this article, please refer to the Version of Record once published for full citation and copyright details, as permissions may be required.

The source of topography across the Cumberland Peninsula, Baffin Island, Arctic Canada: differential exhumation of a North Atlantic rift flank

Scott Jess^{1*}, Randell Stephenson¹, Søren B. Nielsen², Roderick Brown³

¹ School of Geosciences, University of Aberdeen, Aberdeen, AB24 3UE, UK.

² Department of Geoscience, Aarhus University, DK-8000 Aarhus C, Denmark.

³ School of Geographical and Earth Sciences, University of Glasgow, Glasgow, G12 8QQ, UK.

*Correspondence (scott.jess@ucalgary.ca)

Uplift of Baffin Island

Abstract

Elevated topography is evident across the continental margins of the Atlantic. The Cumberland Peninsula, Baffin Island, formed as the result of rifting along the Labrador-Baffin margins in the late Mesozoic and is dominated by low relief high elevation topography. Apatite fission track (AFT) analysis of the landscape previously concluded that the area has experienced a differential protracted cooling regime since the Devonian; however, defined periods of cooling and the direct causes of exhumation were unresolved. This work combines the original AFT data with 98 apatite new (U-Th)/He ages from 16 samples and applies the newly developed 'broken crystals' technique to provide a greater number of thermal constraints for thermal history modelling to better constrain the topographic evolution. The spatial distribution of AFT and AHe ages implies exhumation has been significant toward the SE (Labrador) coastline, while results of thermal modelling outline three notable periods of cooling in the pre-rift (460 Ma – 200 Ma), from syn-rift to present (120 Ma – 0 Ma) and within post-rift (30 Ma – 0 Ma) stages. Pre-rift cooling is interpreted as the result of exhumation of Laurentia, syn-rift cooling as the result of rift flank uplift to the SE and

differential erosion of landscape, while the final post-rift period is likely an artefact of the modelling process. These results suggest the source of the Cumberland Peninsula's modern-day elevated topography is uplift during rifting in the Cretaceous and the isostatic compensation following continuous Mesozoic and Cenozoic differential erosion. This work highlights the how interaction of rift tectonics and isostasy can be the principal source for modern elevated continental margins, while also providing insight into the pre-rift exhumational history of central Laurentia.

Introduction

The continental margins of the Atlantic exhibit elevated coastal topography reaching up to ~3 km in height, yet the source and age of topography remains a contentious issue (Japsen & Chalmers, 2000; Nielsen et al., 2009; Green et al., 2018). The margins of Brazil, Southern Africa, Norway and Greenland are all characterised by high elevation low relief topography, while aspects of the offshore stratigraphy have been interpreted in terms of a fluctuating onshore denudational history (Riis, 1996; Evans, 1997; Japsen, 1998; Chalmers, 2000; Burke & Gunnell, 2008; Cobbold et al., 2010). Various mechanisms have previously been suggested to explain both the onshore and offshore geology: mantle diapirism (Rohrman & van der Beek, 1996), rift flank uplift (Redfield et al., 2005), tectonic rejuvenation (Ksienzyk et al., 2014), far field stress changes (Japsen et al., 2014) and isostasy (Medvedev et al., 2008). However, a clear consensus is yet to be established.

Low temperature thermochronology and thermal history modelling have become vital tools in establishing the onshore denudational and uplift histories of modern passive margins (e.g. Gallagher et al., 1994; Cockburn et al., 2000; Kounov et al., 2009; Wildman et al., 2015), in part due to a lack of direct geological evidence and difficulties integrating onshore and offshore histories. Thermal histories generated from across several continental margins outline the timing and style of cooling or heating to establish periods of exhumation or burial respectively, helping to infer how a landscape has evolved (Gallagher, 1998). Across Greenland and Brazil topography is interpreted to have formed from multiple tectonic uplift

events following the end of rifting, inferred from episodic rapid cooling in thermal histories (Japsen et al., 2006; Japsen et al., 2012; Japsen et al., 2014), while protracted cooling, observed in thermal models from Norway and Southern Africa suggests topography along these margins results from a prolonged denudation across elevated rift flanks (Brown et al., 2000; Hendriks & Andriessen, 2002) or ancient topography (Nielsen et al., 2009). These contrasting interpretations illustrate the contentious debate surrounding the evolution of Atlantic continental margins and highlights the key role thermal history modelling plays in establishing the topographic evolution of continental margins.

The Baffin Mountains, along the NE coastline of Baffin Island (Fig. 1), are an example of low relief landscape at high elevation (~2 km) and, like many other instances from across the Atlantic, the source of this topography remains enigmatic. Early geomorphological research from Baffin Island suggested much of the modern landscape is the result of a peneplain that was uplifted in the late Cenozoic (Cooke, 1931; Mercer, 1956; Bostock, 1970). However, apatite fission track data and thermal history models from the Cumberland Peninsula, SE Baffin Island, show no evidence for uplift in the Cenozoic and are interpreted as the result of protracted erosion since the Devonian (McGregor et al., 2013). The present work attempts to better constrain the thermal history from across the Cumberland Peninsula with the addition of 98 single grain apatite (U-Th)/He ages from 16 samples of the original fission track dataset and, further, utilising the 'broken crystals' approach in one sample to provide greater temporal and thermal resolution (Brown et al., 2013). The resulting spatial data trends and enhanced thermal histories suggest that uplift of the margin occurred during rifting in the late Mesozoic and has since been preserved by isostatic forces, while additional insight into the pre-rift history is also provided.

Geological setting

The geology of the Cumberland Peninsula is dominated by Archaean orthogneisses and amphibolites of the Hoare Bay Group and granulites of the Cumberland batholith that amalgamated as part of the 'Rae Craton Expansion' (~2.0 Ga) (St-Onge et al., 2009). The

collision of five Archaean terranes led to the metamorphism of the original continental shelf sediments of the Hoare Bay Group (1.88 Ga) (St-Onge et al., 2009) and generated the granitic melt of the Cumberland Batholith, now located across the centre of Baffin Island. Subsequent collision with the Superior Craton to the west, as part of the Trans-Hudson Orogeny (~1.8 Ga), combined many early crustal domains together to form the supercontinent of Laurentia (Lewry & Collerson, 1987; St-Onge et al., 2009). Evidence of intra-cratonic subsidence and uplift of Laurentia during the Palaeozoic and Mesozoic is apparent in several localities (Flowers et al., 2012; Zhang et al., 2013; Ault et al., 2013), though is poorly resolved due to a lack of preserved geology.

Extension between eastern Canada and western Greenland is believed to have begun in the Late Triassic and continued through to the Palaeocene (Larson et al., 2009). The geochemistry of igneous intrusions across both margins and observed fault block rotation in the offshore outline three intense periods of rifting in the late Mesozoic and early Cenozoic: Late Jurassic to Early Cretaceous (150 Ma – 130 Ma), Mid Cretaceous (120 Ma – 100 Ma) and Late Cretaceous to Palaeocene (80 Ma – 64 Ma) (Balkwill, 1987; Larsen et al., 2009). Ocean spreading in the region began in the Labrador Sea during the Late Cretaceous and migrated northwards into Baffin Bay in the Palaeocene, aided by the ~700 km long strike-slip Ungava Fault Zone (Funck et al., 2007; Suckro et al., 2013) (Fig. 1). Spreading within Baffin Bay kinematically re-orientated in Late Palaeocene to Early Eocene (N-S to NNW-SSE) (~57-53Ma), coeval to the Eureka Orogeny to the north, and ceased all together in the Late Eocene (~34 Ma) (Oakey & Chalmers, 2012) (Fig. 1).

Rifting led to significant sedimentary basin development across Baffin Bay and the Davis Strait, with several kilometres of deltaic and marine sediments offshore (Chalmers, 2012). Onshore stratigraphic exposure across the Cumberland Peninsula is limited to Cretaceous sands found in half grabens on Durban, Padloping and Quqalluit islands interpreted as the deposits of a major Cretaceous braided river system (Burden & Langille, 1990) (Fig. 1). Sub-aqueous and sub-aerial volcanoclastics and lavas overlie these

Cretaceous sands, onlapping onto the surrounding basement, and are interpreted as the most westerly extent of the West Greenland Igneous Province (Clarke & Upton, 1971) (Fig. 1). Offshore stratigraphy is not well defined, though Cretaceous sands are found just below the sea floor of the NE coastline of the Cumberland Peninsula (MacLean et al., 2014) and ~1 km of Neogene sediments is present off the shelf (Thiebault et al., 1989; Chalmers, 2012). The elevated peneplain across Baffin Island has been proposed to result from uplift in the late Cenozoic (Bostock, 1970), though contemporary studies have suggested these features may be formed through differential erosion across the landscape during glaciation (Egholm et al., 2017; Strunk et al., 2017).

The discernible lack of Mesozoic and Cenozoic rocks makes it difficult to constrain the onshore evolution of the region. Fortunately, the application of apatite low-temperature thermochronology can contribute to our understanding of the region's history.

Methodology

Low temperature thermochronology

In this study thermal histories are generated by the joint inversion of apatite fission track (AFT) and apatite (U-Th)/He (AHe) data (Gallagher et al., 1998). AFT utilises damage trails produced within the crystal lattice of apatite following the fission decay of ^{238}U to establish the age and rate of cooling through the apatite fission track partial annealing zone (PAZ: 120 °C – 60 °C). Central ages utilised in this study were determined through the external detector method (Gleadow et al., 1981), while the style of cooling is established by the distribution of horizontal confined fission track lengths, as residence in the PAZ shortens tracks from their initial size (~16.2 μm) producing a length distribution dependent on a sample's thermal history. AHe utilises the accumulation of ^4He in the apatite grains derived from the alpha decay of ^{238}U , ^{235}U and ^{232}Th at temperatures <70 °C (Wolf et al., 1998). The concentrations of both ^4He and radioactive isotopes are used to determine the time at which the grain was within the helium partial retention zone (HePRZ; 70 °C – 40 °C) (Wolf et al.,

1998; Stockli et al., 2000), providing temporal and thermal constraints on a geological timescale.

From the 20 samples analysed in the initial AFT study (McGregor et al., 2013), 16 were used for whole grain (U-Th)/He analysis and 20 fragmented grains were analysed from one of the youngest AFT samples (Ec8) (Brown et al., 2013). Selecting appropriate apatite grains from metamorphic rocks is difficult due to the high likelihood of ^4He rich inclusions and pitted mineral surfaces, caused by grain boundary interactions at depth (Dempster et al., 2006). Criteria used to ensure that suitable grains were picked included: a euhedral or sub-euhedral morphology, a lack of observable mineral inclusions and good optical clarity to ensure the internal structure of the grain could be observed. Analysis was completed at the London Geochronology Centre where each grain was heated to ~ 650 °C for 120 s using a 25W 808nm diode laser and ^4He measured with a Balzers quadrupole mass spectrometer. Uranium and Thorium measurements were completed through acid digestion and isotope dilution with an Agilent 7700x ICP-MS.

AHe single-grain age dispersion is common in non-orogenic settings due to multiple factors: grain size (Reiners & Farley, 2001), ^4He implantation (Farley et al., 1996), U and Th rich inclusions (Vermeesch et al., 2007), implantation (Gautheron et al., 2012) and radiation damage (Schuster et al., 2006; Flowers et al., 2009; Gautheron., et al., 2009). In an attempt to improve thermal history model precision, the use of fragmented grains on sample Ec8 was employed. Apatite grains commonly break parallel to the c-axis during mineral separation, producing a grain fragment with a specific portion of the helium diffusion profile and calculated ages are either younger or older than the potential 'whole grain' age (Brown et al., 2013). The analysis of >20 fragments of varying lengths from a single rock sample generates a distribution of ages with 'predictable' dispersion that provides a greater number of thermal and temporal constraints for thermal history modelling (Beuchers et al., 2013).

Thermal modelling

Integrated inverse modelling of AFT and AHe data was completed using the transdimensional Bayesian Markov Chain Monte Carlo (MCMC) within QTQt (Gallagher, 2012). This approach samples >200,000 thermal histories, continually assessing the predictions of AFT central age, track distribution and AHe ages against each iteration to ascertain if the prediction has improved and finally producing an 'expected model' that is bound by 95% credibility intervals. This 'expected model' outlines a single thermal history derived from a wide range of possible outcomes and does not forcibly overinterpret the data in the modelling process, producing a thermal history dependent on the joint inversion of both datasets and the quality of the data. Moreover, this approach also permits the application of c-axis correction on AFT track length data (Donelick et al., 1999), greatly improving modelling accuracy, and the resampling of AHe age error which allows for a greater degree of freedom while modelling and objectively discounting single AHe ages that are incompatible with the counterpart AFT data.

As mentioned above, radiation damage within apatite grains can influence AHe ages, producing $\leq 100\%$ dispersion in affected samples. Ongoing recoil of the U and Th decay chain can damage the surrounding crystal lattice creating vacancies that can accommodate ^4He diffused above $\sim 70^\circ\text{C}$ that is then included in analysis, increasing the overall age (Shuster et al., 2006). In an attempt to improve the compatibility of dispersed AHe ages, a radiation damage diffusion model and alternative diffusion parameters are incorporated that treat radiation damage defects similar to fission tracks during a calculated thermal history (Gautheron et al., 2009). Though this may not account for all dispersion within samples, it has been shown to improve AFT and AHe age predictions in comparison to standard apatite diffusion kinetics (e.g. Cogné et al., 2012; Guillaume et al., 2013; Leprêtre et al., 2015; Wildman et al., 2015; Kasanzu, 2017).

Results

Low temperature thermochronology

Fission track central ages (extracted from McGregor et al., 2013) range between 177.4 ± 6.8 Ma and 440.9 ± 22.2 Ma and display a trend of younger ages toward the SE margin (Fig. 2; Fig. 3b) outlining isochrons dipping to the SE-NW (Fig. 3c). Mean track lengths (MTL) range between $12.09 \mu\text{m}$ - $13.27 \mu\text{m}$ (uncorrected) and $13.17 \mu\text{m}$ - $14.22 \mu\text{m}$ (c-axis corrected), with the highest values found across inland and elevated areas, while lower MTLs focus around highly glaciated coastal regions. AFT central ages and MTL against elevation exhibit no obvious trend (Fig. 3a), while a positive correlation is apparent between Cl wt% and AFT central age (Fig. 4d) and absent between the kinetic parameter D_{par} and AFT central age (Fig. 4a). Of the 22 samples, 5 provide chi-squared values of less than 5%, though dispersion of all samples is $<15\%$, suggesting low values are likely determined by less than 20 grains counted or low track densities.

Whole grain AHe ages range between 0.0 Ma and 3.4 Ga for uncorrected ages and 0.0 Ma and 4.6 Ga for corrected ages (Table. 1). Specific removal of ages considered very young (<1 Ma) and those considered very old (>1 Ga) from the dataset produces alternative age ranges; 5.51 Ma and 610.2 Ma (uncorrected) and 8.09 Ma and 690.8 Ma (corrected). Mean sample ages from this altered dataset range between 104.0 Ma and 279.4 Ma (uncorrected) and 123.7 Ma and 329.9 Ma (corrected) and also displays a trend of younger ages toward the SE, similar to that of AFT central ages (Fig. 2; Fig. 3b). Effective uranium concentration ($eU = [U] + 0.235[Th]$) against AHe age shows weak to moderate positive correlations in 11 of the 16 whole grain samples, while equivalent spherical radius and AHe age show weak to moderate positive correlations in 14 of the 16 samples (Fig. 3d). These trends imply that both radiation damage and grain geometry are dominant controls on whole grain ages and suggest many of the samples have spent considerable time within the HePRZ (Reiners & Farley, 2001; Flowers et al., 2009). Grains with anomalously high ages (>1 Ga) imply significant quantities of additional ^4He have entered the diffusion domain, likely

through micro-inclusions or implantation. Very young ages (<1 Ma) can be attributed to the potential accidental selection of zircon instead of apatite or a failure to reach an optimum temperature during ^4He extraction. Fragment (“broken grain”) ages range between 62.6 Ma and 610.1 Ma (uncorrected), and 68.4 Ma and 690.1 Ma (corrected). eU against fragment age also exhibits a weak positive correlation, while fragment length against fragment age displays no obvious trend, again suggesting radiation damage is a principle control on AHe ages.

Examination of both the AFT and AHe data reveals an overlapping of age ranges across several samples, reflecting the extent of dispersion in the data, though AFT central age against mean AHe age does exhibit a moderate positive correlation suggesting some compatibility between the two systems. Notably, dispersion of AHe ages does display a weak positive correlation against AFT central age, implying older AFT central ages may yield wider dispersion in the (U-Th)/He system, conceivably due to thermal histories with extended periods of time within the HePRZ.

Thermal modelling

Thermal histories generated from across the study area exhibit both linear protracted cooling and a variety of cooling episodes stretching from the late Palaeozoic to Late Cenozoic. The study area is divided into three segments (NW, central and SE) and thermal histories can be found in Figure 4 and the supplementary data.

In the NW segment, thermal histories from across Qikiqtarjuaq and the coastline exhibit accelerated cooling from the Cretaceous to present in Ec1, Ec2 and Ec17, with a rate of cooling that varies between 0.4 °C/Myr – 0.8 °C/Myr. A Late Cenozoic cooling episode is also observed in the more elevated Ec13, Ec16, and Ec18 samples, while rates range between 0.7 °C/Myr – 1.5 °C/Myr. Late Palaeozoic/early Mesozoic cooling is exhibited in Ec13 and Ec16 from elevated positions and Ec17 from a low elevation, with cooling rates

spanning 0.4 °C/Myr – 1.1 °C/Myr, while Ec14 and Ec3, the only sample with just AFT data, both exhibit linear protracted cooling with a rate of 0.2 °C/Myr.

In the central segment of the study area, accelerated cooling from the Cretaceous to present is only observed in Ec22, with a cooling rate of 0.5 °C/Myr. A Late Cenozoic cooling episode is also observed in thermal histories from low elevation coastal samples Ec12 and Ec19, both exhibiting a rate of 1 °C/Myr. Accelerated late Palaeozoic/early Mesozoic cooling is observed in low elevation samples Ec19, Ec21 and Ec22 with varying rate of cooling between 0.3 °C/Myr - 1.1 °C/Myr, while linear protracted cooling is observed in the elevated and inland samples Ec20 and Ec23, both exhibiting a rate of 0.2 °C/Myr.

In the SE segment, accelerated cooling from the Cretaceous to present is displayed in the low elevation samples of Ec7 and Ec8, with a rate between 0.6 °C/Myr – 0.8 °C/Myr. A Late Cenozoic cooling episode is also observed in only the low elevation sample Ec5, exhibiting a rate of 1.4 °C/Myr. Additionally, late Mesozoic cooling is also observed in the low elevation Ec7 and Ec8 samples with rates varying between 1.2 °C/Myr – 1.3 °C/Myr, while the elevated Ec10 sample, derived from AFT data alone, exhibits linear protracted cooling with a rate of 0.25 °C/Myr.

Predicted AFT central ages and c-axis corrected track distributions from thermal histories are all modelled within error, with the exception of Ec14, where the central age is calculated from only 4 grains, suggesting the age itself is anomalous. Predictions of whole grain AHe ages varies, with AHe ages younger than the counterpart AFT central ages appropriated replicated, while ages similar to or older than AFT central ages are predicted poorly. Fragment grain ages within sample Ec8 display a similar trend, with younger ages predicted well alongside AFT and whole grain AHe ages, though 5 fragments older than the AFT central age are poorly replicated (Fig. 5).

Discussion

Evolution of the Cumberland Peninsula

The AFT/AHe results and thermal histories from this work suggest the modern topography of the Cumberland Peninsula has been predominantly shaped by surface uplift during rifting in the Cretaceous and subsequent differential denudation. Additionally, insight into the pre-rift history of the region is provided by a collection of thermal histories that imply exhumation of central Laurentia during the late Palaeozoic/early Mesozoic. These results support the conclusions of the original AFT study (McGregor et al., 2013), though improved resolution of the syn-rift and post-rift history has been gained through the addition of AHe data.

Uplift and preservation of the Cumberland Peninsula's topography

The principal source of surface uplift across the Cumberland Peninsula is likely flank uplift during active rifting in the Cretaceous (Fig. 6a). Rift flank uplift of strong, cold lithosphere is a long known and well understood phenomenon (Buck, 1986; Braun & Beaumont, 1989; Weissel & Karner, 1989) and can account for kilometres of rock uplift during the active rifting phase. Spatial trends in the AFT and AHe data exhibit younger ages toward the SE coastline and outline inclined isochrons orientated NW-SE, implying that considerable rock uplift of the SE coastline has occurred (Fig. 3). This is corroborated by the onset of cooling in the Cretaceous, evident in many of the thermal histories from coastal and low elevation samples (Fig. 5), likely the thermal response to exhumation during and following uplift. Exhumation of the region at the time is evident with an erosional contact between syn-rift fluvial sediments and the underlying basement observable across Durban, Padloping and Quqaluit islands (Fig. 1) (Burden & Langille, 1990). Moreover, this proposed rift flank uplift of the SE margin accounts for the higher modern topography observed toward the SE of the study area, indicative of a major erosional escarpment (Fig. 6a) (Mayer, 1986; Tucker & Slingerland, 1994), that would have redirected drainage systems in the study area NE into Baffin Bay during rifting.

After the end of rifting in the Early Palaeocene, differential erosion of the rift flank likely continued throughout the post-rift stage. Many of the thermal histories from across the margin outline continuous cooling throughout the Cenozoic, with cooling rates themselves varying between high and low elevations, implying differential denudation was evident across the landscape (Fig. 5). This last point is implied by the modern fjordal distribution, which mimics the characteristics of dendritic drainage patterns (Fig. 6b), suggesting later glaciers may have overprinted rift-related fluvial systems through topographically constrained glacial flow. Two dendritic glacial drainage systems are observable within the modern landscape (Fig. 6b), extracted through the application of flow accumulation analysis, an analytical approach that determines overland fluid flow pathways based on digital elevation models (Jenson & Domingue, 1988). These systems flow SW-NE into Baffin Bay at Padloping Island and Qikiqtarjuaq, overlapping the location of the aforementioned Cretaceous river sediments (Fig. 6b) and suggest they may outline the redirected fluvial systems that formed during surface uplift in the Cretaceous. Glacial overprinting of these river valleys is likely to have occurred during the Neogene and Quaternary, inheriting the dendritic drainage pattern through the process of selective linear erosion that over-deepened pre-glacial network, analogous to similar examples from Greenland (Bamber et al., 2013; Cooper et al., 2016).

This interpretation of the post-rift evolution of the Cumberland Peninsula does fail to account for the final period of cooling observed in a number of thermal histories. This cooling (~30 Ma – 0 Ma) occurs outside the temperature sensitivity ranges of both the AFT and AHe systems, implying it may be an artefact of the modelling process due to a drop in surface temperatures in the Late Cenozoic (~10 - 20 °C). Climatic cooling at high latitudes is thought to have occurred at the Eocene-Oligocene boundary (~33 Ma) (Eldrett et al., 2009; Bernard et al., 2016), while the onset of glaciation across NE Canada is believed to have occurred in the Miocene (Ehlers & Gibbard, 2007). A significant drop in surface temperature following a

sample's exit from the PAZ and HePRZ would result in a significant cooling event being present in thermal models due to the enforced present-day thermal constraint of 0 °C.

In addition to defining the region's uplift history, results from thermal modelling also provide insight into the exhumation of the Cumberland Peninsula prior to rifting, supporting the conclusions of McGregor et al. (2013). A record of the geology during this time is absent in the study area, though cooling during the late Palaeozoic/early Mesozoic in a collection of thermal models (Fig. 5) reiterates the conclusions of numerous studies that infer widespread exhumation of Laurentia during the same period (Pysklywec and Mitrovica, 2000; Flowers et al., 2012; Ault et al., 2013; McGregor et al., 2013). Stratigraphic evidence of exhumation from this time is limited in the immediate surroundings, though much larger basins across the craton's periphery, such as the Sverdrup Basin, do show evidence of terrestrial systems originating from across the Laurentia (Patchett et al., 2004; Midwinter et al., 2016). This could suggest large-scale fluvial systems flowed across Laurentia toward the Sverdrup Basin during the late Palaeozoic and early Mesozoic (Fig. 6c), providing a viable mechanism for cooling across the Cumberland Peninsula prior to later rifting.

Preservation of the Cumberland Peninsula's topography

The results presented above suggest the origin of high topography across SE Baffin Island occurred during rifting in the Cretaceous followed by continuous fluvial and glacial erosion in the Cenozoic. This interpretation provides an explanation for much of the thermochronology, geomorphology and stratigraphy, though does not explain how the modern topography itself remains elevated at present (≤ 2 km).

A mechanism that can explain elevated topography in regions of continuous exhumation is isostatic feedback from the lithosphere following differential denudation (Stephenson & Lambeck, 1985; Gilchrist & Summerfield, 1991; Tucker & Slingerland, 1994; Rouby et al., 2013). Surface uplift across Greenland and Norway in response to erosional unloading of the lithosphere during glaciation has been shown to reach up to ~1000 m

(Medvedev et al., 2008; Medvedev et al., 2013; Medvedev & Hartz, 2015), implying a similar effect may have occurred across the Cumberland Peninsula. The extent of glacial erosion across the margin is evident in the modern geomorphology, suggesting significant volumes of rock have been removed, in turn driving a considerable isostatic response. To test the degree to which erosion has driven surface uplift in the region, a simple 2D flexural model of the isostatic response was considered, in which the modern fjords are refilled with eroded material (Fig. 7) (see also Supplementary Data), analogous to the work of Medvedev et al. (2013). Results show an increase in maximum elevation of 91 m and a drop in average elevation of 209 m, outlining how differential denudation of the lithosphere will produce rock column uplift and effectively preserve the highest topography (Fig. 7). This model provides a simple demonstration of the first order role isostasy plays within the exhumation of passive margins and how it preserves the elevated rift flank topography of the Cumberland Peninsula.

Implications for Atlantic continental margins

The origin and age of topography across continental passive margins has been a widely debated topic within the geological community for over a century (e.g. Geikie, 1901; Reusch, 1901; Steers et al., 1948; Holtedahl, 1958; Mörner, 1979; Japsen & Chalmers, 2000; Anell et al., 2009; Nielsen et al., 2009; Green et al., 2013; Green et al., 2018; Japsen et al., 2018). Both post-rift tectonism and isostatic compensation driven by differential erosion are cited as possible sources of elevated topography across Greenland, Norway, Brazil and South Africa (Brown et al., 2000; Hendriks & Andriessen, 2002; Japsen et al., 2006; Nielsen et al., 2009; Japsen et al., 2012; Japsen et al., 2014). The contentious interpretation of inferred peneplains as direct indicators of surface uplift and the lack of an obvious cause of uplift following the end of rifting make it difficult to support the former theory of passive margin topographic generation. Instead, the conclusions of this work support the latter of the two theories as the rift-related topography of the Cumberland Peninsula is interpreted to have been preserved by differential exhumation of the rift flank and isostatic compensation. Moreover, the trend in AFT central ages suggesting the flexure of the

lithosphere is comparable to those observed across Southern Norway (Redfield et al., 2005), West Greenland (Redfield, 2010) and Brazil (Gallagher et al., 1995), highlighting the probable first order control rifting has on passive margin topography. The similarity in these results would suggest topography along many Atlantic passive margins may be explained through the interaction of rift tectonics, differential exhumation and isostatic compensation rather than post-rift tectonism.

Previous thermochronological studies from passive margins in the Baffin Bay region display similar trends in cooling, providing regional consistency to this study's interpretation. Across the continental margins of Baffin Bay and the Labrador Sea AFT and AHe ages appear similar to those reported here (Hendriks et al., 1993; Japsen et al., 2006; McDannell et al., 2019; Jess et al. 2019), while the interpretation of rift related uplift and differential erosion shaping the landscape is comparable (Hendriks et al., 1993; Jess et al. 2019). AFT data from both Newfoundland and West Greenland are interpreted to suggest the modern topography is the result of rift-related uplift (Hendriks et al., 1993; Jess et al., 2019), while low rates of exhumation during the Cenozoic are inferred from thermal modelling of both AFT and AHe data (Jess et al. 2018). Collectively this suggests much of the topography observed across the wider region is likely the result of preserved rift-related uplift, such that both margins have evolved according to a single unifying conceptual model that does not require the intervention of post-rift uplift.

Dispersion in AHe ages

The application of the 'broken crystal' technique within Ec8 improves modelling results through the inclusion of additional thermal information, though robust joint inverse thermal history modelling of other samples is made difficult by high levels of whole grain age dispersion (Fig. 5; Ec12 & Ec16). The radiation damage model and diffusion parameters applied to thermal histories (Gautheron et al., 2009) improves AHe age predictions relative to standard apatite diffusion parameters (Farley, 2000), though does not produce suitable predictions for a collection of the AHe ages. This implies other underlying factors, which are

not accounted for in the modelling methodology (e.g. mineral inclusions, zonation, implantation), and the developing understanding of the AHe system may hinder effective prediction of highly dispersed AHe ages in the passive margin settings. Moreover, data used to validate and justify radiation damage models commonly differ to those found along passive margin settings: (i) sedimentary samples being commonly used, (ii) AFT ages rarely exceeding 200 Ma and (iii) a lack of well documented stratigraphy commonly in place to improve modelling constraints (Flowers et al., 2009; Gautheron et al., 2009; Gautheron et al., 2013). Accordingly, the geological setting of the Cumberland Peninsula and lengthy periods spent within the HePRZ (>100 Myr) hinder the application of current radiation damage models, implying further work on the topic in passive margin settings is essential.

Summary and conclusions

Low-temperature thermochronology and thermal history modelling help to outline how the landscape of the Cumberland Peninsula, Baffin Island, has evolved through the Mesozoic and Cenozoic. Results from this work imply that the modern topography of the margin is derived from rift-flank uplift in the Mesozoic and isostatic flexure in response to erosion thereafter.

Rift-flank uplift of the margin is implied by the spatial distribution of AFT and AHe ages, the onset of accelerated cooling in the Cretaceous and the modern geomorphology. It is suggested that during rifting, uplift of the SE coastline of Baffin Island formed a considerable elevated landscape and escarpment that forced erosive fluvial systems NE into Baffin Bay. These fluvial drainage patterns may still be observable in the modern geomorphology as selective linear erosion during glaciation likely over-deepened many of the pre-glacial valleys to form the modern fjords. Two outcomes of this differential erosion include the preservation of elevated topography and the removal of vast quantities of rock from the upper crust, prompting a positive isostatic response across the peninsula. In addition to constraining the timing uplift, insight into the pre-rift history of the region is provided, with widespread cooling in the late Palaeozoic and early Mesozoic linked to

exhumation of Laurentia, in accordance with similar interpretations from across the Cumberland Peninsula and northern Canada. These results and interpretations provide a suitable account of the Cumberland Peninsula region's uplift history and determine that its modern elevated topography is a remnant rift flank, augmented by differential erosion and isostasy.

Acknowledgements

Eoin McGregor is sincerely thanked for the collection of samples, while Andy Carter and James Schwanethal are also thanked for their assistance in sample preparation and analysis. Thanks is also given to Yanni Gunnell, James Spotila and Lisel Currie for their constructive comments and reviews. The work reported here was conducted during a PhD study undertaken as part of the Natural Environment Research Council (NERC) Centre for Doctoral Training (CDT) in Oil & Gas [grant number NEM00578X/1] and was sponsored by the University of Aberdeen.

References

- Allmendinger, R.W., Cardozo, N. and Fisher, D.M., 2011. *Structural geology algorithms: Vectors and tensors*. Cambridge University Press.
- Anell, I., Thybo, H. and Artemieva, I.M., 2009. Cenozoic uplift and subsidence in the North Atlantic region: Geological evidence revisited. *Tectonophysics*, 474(1-2), pp.78-105.
- Ault, A.K., Flowers, R.M. and Bowring, S.A., 2013. Phanerozoic surface history of the Slave craton. *Tectonics*, 32(5), pp.1066-1083.
- Bamber, J.L., Siegert, M.J., Griggs, J.A., Marshall, S.J. and Spada, G., 2013. Paleofluvial mega-canyon beneath the central Greenland ice sheet. *Science*, 341(6149), pp.997-999.

- Bernard, T., Steer, P., Gallagher, K., Szulc, A., Whitham, A. and Johnson, C., 2016. Evidence for Eocene–Oligocene glaciation in the landscape of the East Greenland margin. *Geology*, 44(11), pp.895-898.
- Beucher, R., Brown, R.W., Roper, S., Stuart, F. and Persano, C., 2013. Natural age dispersion arising from the analysis of broken crystals: Part II. Practical application to apatite (U–Th)/He thermochronometry. *Geochimica et Cosmochimica Acta*, 120, pp.395-416.
- Blakey, R.C. and Wong, T.E., 2003, August. Carboniferous–Permian paleogeography of the assembly of Pangaea. In *Proceedings of the XVth International Congress on Carboniferous and Permian Stratigraphy. Utrecht* (Vol. 10, p. 16).
- Brown, R.W., Beucher, R., Roper, S., Persano, C., Stuart, F. and Fitzgerald, P., 2013. Natural age dispersion arising from the analysis of broken crystals. Part I: Theoretical basis and implications for the apatite (U–Th)/He thermochronometer. *Geochimica et Cosmochimica Acta*, 122, pp.478-497.
- Brown, R.W., Gallagher, K., Gleadow, A.J. and Summerfield, M.A., 2000. Morphotectonic evolution of the South Atlantic margins of Africa and South America. *Geomorphology and global tectonics*, pp.255-281.
- Burden, E.T. and Langille, A.B., 1990. Stratigraphy and sedimentology of Cretaceous and Paleocene strata in half-grabens on the southeast coast of Baffin Island, Northwest Territories. *Bulletin of Canadian Petroleum Geology*, 38(2), pp.185-196.

- Burke, K. and Gunnell, Y., 2008. *The African erosion surface: a continental-scale synthesis of geomorphology, tectonics, and environmental change over the past 180 million years. Geological Society of America Memoir*, 201, pp 72.
- Chalmers, J.A., 2000. Offshore evidence for Neogene uplift in central West Greenland. *Global and Planetary Change*, 24(3), pp. 311-318.
- Chalmers, J.A., 2012. Labrador Sea, Davis Strait, and Baffin Bay. In *Regional Geology and Tectonics: Phanerozoic Passive Margins, Cratonic Basins and Global Tectonic Maps* (pp. 384-435).
- Clarke, D.B. and Upton, B.G.J., 1971. Tertiary basalts of Baffin Island: field relations and tectonic setting. *Canadian Journal of Earth Sciences*, 8(2), pp.248-258.
- Cobbold, P.R., Chiossi, D., Green, P.F., Jaspén, P. and Bonow, J., 2010. Compressional reactivation of the Atlantic Margin of Brazil: Structural styles and consequences for hydrocarbon exploration. *Search Discovery*, 30114.
- Cockburn, H.A.P., Brown, R.W., Summerfield, M.A. and Seidl, M.A., 2000. Quantifying passive margin denudation and landscape development using a combined fission-track thermochronology and cosmogenic isotope analysis approach. *Earth and Planetary Science Letters*, 179(3-4), pp.429-435.
- Cogné, N., Gallagher, K., Cobbold, P.R., Riccomini, C. and Gautheron, C., 2012. Post-breakup tectonics in southeast Brazil from thermochronological data and combined inverse-forward thermal history modeling. *Journal of Geophysical Research: Solid Earth*, 117(B11), 1 – 16.

- Cooper, M.A., Michaelides, K., Siegert, M.J. and Bamber, J.L., 2016. Paleofluvial landscape inheritance for Jakobshavn Isbræ catchment, Greenland. *Geophysical Research Letters*, 43(12), pp.6350-6357.
- Dempster, T.J., Campanile, D. and Holness, M.B., 2006. Imprinted textures on apatite: A guide to paleoporosity and metamorphic recrystallization. *Geology*, 34(11), pp.897-900.
- Dodson, M.H., 1973. Closure temperature in cooling geochronological and petrological systems. *Contributions to Mineralogy and Petrology*, 40(3), pp.259-274.
- Donelick, R.A., Ketcham, R.A. and Carlson, W.D., 1999. Variability of apatite fission-track annealing kinetics: II. Crystallographic orientation effects. *American Mineralogist*, 84(9), pp.1224-1234.
- Ehlers, J. and Gibbard, P.L., 2007. The extent and chronology of Cenozoic global glaciation. *Quaternary International*, 164, pp.6-20.
- Eldrett, J.S., Greenwood, D.R., Harding, I.C. and Huber, M., 2009. Increased seasonality through the Eocene to Oligocene transition in northern high latitudes. *Nature*, 459(7249), p.969.
- Evans, D.J., 1997. Estimates of the eroded overburden and the Permian–Quaternary subsidence history of the area west of Orkney. *Scottish Journal of Geology*, 33(2), pp.169-181.
- Farley, K.A., 2000. Helium diffusion from apatite: General behavior as illustrated by Durango fluorapatite. *Journal of Geophysical Research: Solid Earth*, 105(B2), pp.2903-2914.

- Farley, K.A., Wolf, R.A. and Silver, L.T., 1996. The effects of long alpha-stopping distances on (U-Th)/He ages. *Geochimica et Cosmochimica Acta*, 60(21), pp.4223-4229.
- Flowers, R.M., Ault, A.K., Kelley, S.A., Zhang, N. and Zhong, S., 2012. Epeirogeny or eustasy? Paleozoic–Mesozoic vertical motion of the North American continental interior from thermochronometry and implications for mantle dynamics. *Earth and Planetary Science Letters*, 317, pp.436-445.
- Flowers, R.M., Ketcham, R.A., Shuster, D.L. and Farley, K.A., 2009. Apatite (U–Th)/He thermochronometry using a radiation damage accumulation and annealing model. *Geochimica et Cosmochimica Acta*, 73(8), pp.2347-2365.
- Funck, T., Jackson, H.R., Loudon, K.E. and Klingelhöfer, F., 2007. Seismic study of the transform-rifted margin in Davis Strait between Baffin Island (Canada) and Greenland: What happens when a plume meets a transform. *Journal of Geophysical Research: Solid Earth*, 112(B4), 1 - 22.
- Gallagher, K. and Brown, R., 1997. The onshore record of passive margin evolution. *Journal of the Geological Society*, 154(3), pp.451-457.
- Gallagher, K., 2012. Transdimensional inverse thermal history modeling for quantitative thermochronology. *Journal of Geophysical Research: Solid Earth*, 117(B2), 1 - 16.
- Gallagher, K., Brown, R. and Johnson, C., 1998. Fission track analysis and its applications to geological problems. *Annual Review of Earth and Planetary Sciences*, 26(1), pp.519-572.

- Gallagher, K., Brown, R. and Johnson, C., 1998. Fission track analysis and its applications to geological problems. *Annual Review of Earth and Planetary Sciences*, 26(1), pp.519-572.
- Gallagher, K., Hawkesworth, C.J. and Mantovani, M.S.M., 1994. The denudation history of the onshore continental margin of SE Brazil inferred from apatite fission track data. *Journal of Geophysical Research: Solid Earth*, 99(B9), pp.18117-18145.
- Gautheron, C., Tassan-Got, L., Barbarand, J. and Pagel, M., 2009. Effect of alpha-damage annealing on apatite (U–Th)/He thermochronology. *Chemical Geology*, 266(3-4), pp.157-170.
- Gautheron, C., Tassan-Got, L., Ketcham, R.A. and Dobson, K.J., 2012. Accounting for long alpha-particle stopping distances in (U–Th–Sm)/He geochronology: 3D modeling of diffusion, zoning, implantation, and abrasion. *Geochimica et Cosmochimica Acta*, 96, pp.44-56.
- Geikie, A., 1901. The scenery of Scotland viewed in connection with its physical geology. Macmillan, London, pp 540.
- Gibling, M.R., Calder, J.H., Ryan, R., Poll, H.W.V.D. and Yeo, G.M., 1992. Late Carboniferous and early Permian drainage patterns in Atlantic Canada. *Canadian Journal of Earth Sciences*, 29(2), pp.338-352.
- Gibling, M.R., Culshaw, N., Rygel, M.C. and Pascucci, V., 2008. The Maritimes Basin of Atlantic Canada: basin creation and destruction in the collisional zone of Pangea. *Sedimentary Basins of the World*, 5, pp.211-244.

- Green, P.F., Japsen, P., Chalmers, J.A., Bonow, J.M. and Duddy, I.R., 2018. Post-breakup burial and exhumation of passive continental margins: Seven propositions to inform geodynamic models. *Gondwana Research*, 53, pp.58-81.
- Green, P.F., Lidmar-Bergström, K., Japsen, P., Bonow, J.M. and Chalmers, J.A., 2013. Stratigraphic landscape analysis, thermochronology and the episodic development of elevated, passive continental margins. *Geological Survey of Denmark & Greenland Bulletin*, (30), pp. 150.
- Guillaume, B., Gautheron, C., Simon-Labric, T., Martinod, J., Roddaz, M. and Douville, E., 2013. Dynamic topography control on Patagonian relief evolution as inferred from low temperature thermochronology. *Earth and Planetary Science Letters*, 364, pp.157-167.
- Hadlari, T., Midwinter, D., Galloway, J.M., Dewing, K. and Durbano, A.M., 2016. Mesozoic rift to post-rift tectonostratigraphy of the Sverdrup Basin, Canadian Arctic. *Marine and Petroleum Geology*, 76, pp.148-158.
- Hendriks, B.W. and Andriessen, P.A., 2002. Pattern and timing of the post-Caledonian denudation of northern Scandinavia constrained by apatite fission-track thermochronology. *Geological Society, London, Special Publications*, 196(1), pp.117-137.
- Holtedahl, H., 1958. Some remarks on geomorphology of continental shelves off Norway, Labrador, and southeast Alaska. *The Journal of Geology*, 66(4), pp.461-4671.

- Japsen, P., 1998. Regional velocity-depth anomalies, North Sea Chalk: a record of overpressure and Neogene uplift and erosion. *American Association of Petroleum Geologists Bulletin*, 82(11), pp.2031-2074.
- Japsen, P., Bonow, J.M., Green, P.F., Chalmers, J.A. and Lidmar-Bergström, K., 2006. Elevated, passive continental margins: Long-term highs or Neogene uplifts? New evidence from West Greenland. *Earth and Planetary Science Letters*, 248(1), pp. 330-339.
- Japsen, P., Bonow, J.M., Green, P.F., Cobbold, P.R., Chiossi, D., Lilletveit, R., Magnavita, L.P. and Pedreira, A., 2012. Episodic burial and exhumation in NE Brazil after opening of the South Atlantic. *Geological Society of America Bulletin*, 124(5-6), pp.800-816.
- Japsen, P., Green, P.F., Bonow, J.M., Nielsen, T.F. and Chalmers, J.A., 2014. From volcanic plains to glaciated peaks: Burial, uplift and exhumation history of southern East Greenland after opening of the NE Atlantic. *Global and Planetary Change*, 116, pp.91-114.
- Japsen, P., Green, P.F., Chalmers, J.A. and Bonow, J.M., 2018. Mountains of southernmost Norway: uplifted Miocene peneplains and re-exposed Mesozoic surfaces. *Journal of the Geological Society*, 175(5), pp.721-741.
- Jess, S., Stephenson, R. and Brown, R., 2018. Evolution of the central West Greenland margin and the Nuussuaq Basin: Localised basin uplift along a stable continental margin proposed from thermochronological data. *Basin Research*, 30(6), pp.1230-1246.
- Jess, S., Stephenson, R., Roberts, D.H. and Brown, R., 2019. Differential erosion of a Mesozoic rift flank: Establishing the source of topography across Karrat,

central West Greenland. *Geomorphology*,
doi.org/10.1016/j.geomorph.2019.02.026.

Kasanzu, C.H., 2017. Apatite fission track and (U-Th)/He thermochronology from the Archean Tanzania Craton: Contributions to cooling histories of Tanzanian basement rocks. *Geoscience Frontiers*, 8(5), pp.999-1007.

Kounov, A., Viola, G., De Wit, M. and Andreoli, M.A.G., 2009. Denudation along the Atlantic passive margin: new insights from apatite fission-track analysis on the western coast of South Africa. *Geological Society, London, Special Publications*, 324(1), pp.287-306.

Ksienzyk, A.K., Dunkl, I., Jacobs, J., Fossen, H. and Kohlmann, F., 2014. From orogen to passive margin: constraints from fission track and (U-Th)/He analyses on Mesozoic uplift and fault reactivation in SW Norway. *Geological Society, London, Special Publications*, 390, pp.SP390-27.

Larsen, L.M., Heaman, L.M., Creaser, R.A., Duncan, R.A., Frei, R. and Hutchison, M., 2009. Tectonomagmatic events during stretching and basin formation in the Labrador Sea and the Davis Strait: evidence from age and composition of Mesozoic to Palaeogene dyke swarms in West Greenland. *Journal of the Geological Society*, 166(6), pp.999-1012.

Leprêtre, R., Missenard, Y., Barbarand, J., Gautheron, C., Saddiqi, O. and Pinna-Jamme, R., 2015. Postrift history of the eastern central Atlantic passive margin: Insights from the Saharan region of South Morocco. *Journal of Geophysical Research: Solid Earth*, 120(6), pp.4645-4666.

- MacLean, B., Williams, G., Zhang, S. and Haggart, J.W., 2014. New insights into the stratigraphy and petroleum potential of the Baffin Shelf's Cretaceous rocks. *Bulletin of Canadian Petroleum Geology*, 62(4), pp.289-310.
- Mayer, L.A.R.R.Y., 1986. Tectonic geomorphology of escarpments and mountain fronts. *Active Tectonics*, pp.125-135.
- McDannell, K.T., Schneider, D.A., Zeitler, P.K., O'Sullivan, P.B. and Issler, D.R., 2019. Reconstructing deep - time histories from integrated thermochronology: An example from southern Baffin Island, Canada. *Terra Nova*. <https://doi.org/10.1111/ter.12386>
- McGregor, E.D., Nielsen, S.B., Stephenson, R.A., Petersen, K.D. and MacDonald, D.I.M., 2013. Long-term exhumation of a Palaeoproterozoic orogen and the role of pre-existing heterogeneous thermal crustal properties: a fission-track study of SE Baffin Island. *Journal of the Geological Society*, 170(6), pp.877-891.
- Medvedev, S. and Hartz, E.H., 2015. Evolution of topography of post-Devonian Scandinavia: Effects and rates of erosion. *Geomorphology*, 231, pp.229-245.
- Medvedev, S., Hartz, E.H. and Podladchikov, Y.Y., 2008. Vertical motions of the fjord regions of central East Greenland: impact of glacial erosion, deposition, and isostasy. *Geology*, 36(7), pp.539-542.
- Medvedev, S., Souche, A. and Hartz, E.H., 2013. Influence of ice sheet and glacial erosion on passive margins of Greenland. *Geomorphology*, 193, pp.36-46.
- Miller, E.L., Toro, J., Gehrels, G., Amato, J.M., Prokopiev, A., Tuchkova, M.I., Akinin, V.V., Dumitru, T.A., Moore, T.E. and Cecile, M.P., 2006. New insights into

Arctic paleogeography and tectonics from U-Pb detrital zircon geochronology. *Tectonics*, 25(3), pp 1 - 19

Mörner, N.A., 1979. The Fennoscandian uplift and Late Cenozoic geodynamics: geological evidence. *GeoJournal*, 3(3), pp.287-318.

Nielsen, S.B., Gallagher, K., Leighton, C., Balling, N., Svenningsen, L., Jacobsen, B.H., Thomsen, E., Nielsen, O.B., Heilmann-Clausen, C., Egholm, D.L. and Summerfield, M.A., 2009. The evolution of western Scandinavian topography: a review of Neogene uplift versus the ICE (isostasy–climate–erosion) hypothesis. *Journal of Geodynamics*, 47(2-3), pp.72-95.

Oakey, G.N. and Chalmers, J.A., 2012. A new model for the Paleogene motion of Greenland relative to North America: plate reconstructions of the Davis Strait and Nares Strait regions between Canada and Greenland. *Journal of Geophysical Research: Solid Earth*, 117(B10), 1 - 28.

Omma, J.E., Pease, V. and Scott, R.A., 2011. U–Pb SIMS zircon geochronology of Triassic and Jurassic sandstones on northwestern Axel Heiberg Island, northern Sverdrup Basin, Arctic Canada. *Geological Society, London, Memoirs*, 35(1), pp.559-566.

Patchett, P.J., Embry, A.F., Ross, G.M., Beauchamp, B., Harrison, J.C., Mayr, U., Isachsen, C.E., Rosenberg, E.J. and Spence, G.O., 2004. Sedimentary cover of the Canadian Shield through Mesozoic time reflected by Nd isotopic and geochemical results for the Sverdrup Basin, Arctic Canada. *The Journal of Geology*, 112(1), pp.39-57.

Pilkington, M., 1991. Mapping elastic lithospheric thickness variations in Canada. *Tectonophysics*, 190(2-4), pp.283-297.

- Pinet, N., Lavoie, D., Dietrich, J., Hu, K. and Keating, P., 2013. Architecture and subsidence history of the intracratonic Hudson Bay Basin, northern Canada. *Earth-Science Reviews*, 125, pp.1-23.
- Pysklywec, R.N. and Mitrovica, J.X., 2000. Mantle flow mechanisms of epeirogeny and their possible role in the evolution of the Western Canada Sedimentary Basin. *Canadian Journal of Earth Sciences*, 37(11), pp.1535-1548.
- Redfield, T.F., Braathen, A., Gabrielsen, R.H., Osmundsen, P.T., Torsvik, T.H. and Andriessen, P.A.M., 2005. Late Mesozoic to early Cenozoic components of vertical separation across the Møre–Trøndelag Fault Complex, Norway. *Tectonophysics*, 395(3-4), pp.233-249.
- Reiners, P.W. and Farley, K.A., 2001. Influence of crystal size on apatite (U–Th)/He thermochronology: an example from the Bighorn Mountains, Wyoming. *Earth and Planetary Science Letters*, 188(3-4), pp.413-420.
- Reusch, H., 1901. Some contributions towards an understanding of the manner in which the valleys and mountains of Norway were formed. *NGU Yearbook 1900*, pp.124-263.
- Riis, F., 1996. Quantification of Cenozoic vertical movements of Scandinavia by correlation of morphological surfaces with offshore data. *Global and Planetary Change*, 12(1), pp. 331-357.
- Rohrman, M. and van der Beek, P., 1996. Cenozoic postrift domal uplift of North Atlantic margins: an asthenospheric diapirism model. *Geology*, 24(10), pp. 901-904.

- Shuster, D.L., Flowers, R.M. and Farley, K.A., 2006. The influence of natural radiation damage on helium diffusion kinetics in apatite. *Earth and Planetary Science Letters*, 249(3-4), pp.148-161.
- Steers, J.A., 1948. Twelve years' measurement of accretion on Norfolk salt marshes. *Geological Magazine*, 85(3), pp.163-166.
- Stephenson, R. and Lambeck, K., 1985. Erosion - isostatic rebound models for uplift: an application to south - eastern Australia. *Geophysical Journal of the Royal Astronomical Society*, 82(1), pp.31-55.
- Stockli, D.F., Farley, K.A. and Dumitru, T.A., 2000. Calibration of the apatite (U-Th)/He thermochronometer on an exhumed fault block, White Mountains, California. *Geology*, 28(11), pp.983-986.
- St-Onge, M.R., van Gool, J.A., Garde, A.A. and Scott, D.J., 2009. Correlation of Archaean and Palaeoproterozoic units between northeastern Canada and western Greenland: constraining the pre-collisional upper plate accretionary history of the Trans-Hudson orogen. *Geological Society, London, Special Publications*, 318(1), pp. 193-235.
- Suckro, S.K., Gohl, K., Funck, T., Heyde, I., Schreckenberger, B., Gerlings, J. and Damm, V., 2013. The Davis Strait crust—a transform margin between two oceanic basins. *Geophysical Journal International*, 193(1), pp.78-97.
- Thiébault, F., Cremer, M., Debrabant, P., Foulon, J., Nielsen, O.B. and Zimmerman, H., 1989. Analysis of sedimentary facies, clay mineralogy, and geochemistry of the Neogene-Quaternary sediments in Site 645, Baffin Bay. In *Proceedings Ocean Drilling Program. Scientific Results* (Vol. 105, pp. 83-100).

- Tucker, G.E. and Slingerland, R.L., 1994. Erosional dynamics, flexural isostasy, and long-lived escarpments: A numerical modeling study. *Journal of Geophysical Research: Solid Earth*, 99(B6), pp.12229-12243.
- Vermeesch, P., Seward, D., Latkoczy, C., Wipf, M., Günther, D. and Baur, H., 2007. α -Emitting mineral inclusions in apatite, their effect on (U–Th)/He ages, and how to reduce it. *Geochimica et Cosmochimica Acta*, 71(7), pp.1737-1746.
- Wildman, M., Brown, R., Watkins, R., Carter, A., Gleadow, A. and Summerfield, M., 2015. Post break-up tectonic inversion across the southwestern cape of South Africa: New insights from apatite and zircon fission track thermochronometry. *Tectonophysics*, 654, pp.30-55.
- Wolf, R.A., Farley, K.A. and Kass, D.M., 1998. Modeling of the temperature sensitivity of the apatite (U–Th)/He thermochronometer. *Chemical Geology*, 148(1-2), pp.105-114.

Figure and Table Captions

(Figure. 1) Geological map highlighting the onshore geology of the study area, offshore geology of the surrounding region and sample locations and names. Two Proterozoic groups make up the majority of the Cumberland Peninsula (Cumberland Batholith and Hoare Bay Group) and underlie all sampling sites. Samples range in elevation from 0 m to 840 m, stretching across much of the NE coast and reach up to ~60 km inland. This sampling strategy helps establish the denudational history of the heavily glaciated NE coast. Cross-section X and X' is shown in Fig 3c. Offshore, the geology is dominated by Mesozoic and Cenozoic sediments and Palaeogene volcanics. Ocean crust overlies both the Labrador Sea and Baffin Bay, separated by the transpressional Ungava Fault Zone, which is thought to be composed of stretched and intruded igneous crust (map adapted from Oakey & Chalmers (2012)). Locations on map: (Qk) Qikiqtarjuaq, (Ql) Quqalluit, (P) Padloping Island and (D) Durban Island.

(Figure. 2) Topographic map of the Cumberland Peninsula, including AFT and mean AHe ages for given samples. Mean AHe ages are displayed in italics, sample locations are exhibited with the same symbols used in Figure. 3c and letters in superscript highlight the respective sub-sample.

(Figure. 3) Spatial trends of AFT and mean uncorrected AHe ages. (a) Age against elevation exhibits weak positive trends from both AFT and AHe, though there are high levels of scattering, suggesting thermal histories vary greatly across the study area and that elevation is not a primary control on age. (b) Distance from the SE margin (Davis Strait) against age shows a moderate positive correlation for both AFT and mean AHe ages similar to many passive margins, implying that cooling is greater toward the SE and that the opening of Davis Strait may have had a significant effect on the thermal regime of the study area. (c) Sample central ages outline dipping isochrons toward the SE margin suggesting higher rates of rock exhumation or rift flank uplift towards Davis Strait. Ec14 (highlighted with *) is

identified as an outlier due to the sample's young age, a result of only 4 grains being counted.

(Figure. 4) Plots of AFT central ages against compositional and kinetic data and AHe whole grain (2T) and fragment (1T) ages against compositional and geometric data. (a) Dpar against AFT central age shows no obvious trend suggesting it is not a principle control on fission track annealing. (b) [eU] against AHe age in samples Ec2 (NW), Ec7 (SE) and Ec20 (central) displays positive correlations, though higher [eU] values do generally produce higher AHe ages, implying that additional ^4He has accumulated in the grain due to radiation damage. (c) [eU] against AHe fragment age exhibits a weak positive correlation where higher [eU] values have higher AHe ages, with the exception of the two highest [eU] values (>80 ppm), suggesting that radiation damage is a principal control on these ages. (d) Cl wt% against AFT central age shows a weak positive correlation, suggesting that the Cl content in the apatite grains may lower the annealing rate producing older ages. (e) Equivalent grain radius against AHe ages in samples Ec2 (NW), Ec7 (SE) and Ec20 (central) displays positive trends suggesting that diffusion domain size plays a notable role in the final AHe age. (f) Fragment length against AHe fragment age exhibits no obvious trend, implying that the size of diffusion domain is negligible in the final AHe fragment age.

(Figure. 5) Thermal histories from across the Cumberland Peninsula. Expected thermal histories are shown as black lines, while the grey shaded area represents the 95 % confidence interval on either side of the expected history. Data predictions are shown as graphs of observed age against predicted age (\bullet = AFT; \blacktriangle = AHe) and the fit of predicted track distribution against a histogram of track lengths. Moreover, the timing of active rifting in the region (150 Ma - 64 Ma) is indicated by grey boxes in each thermal history. Ec7: thermal history shows two periods of cooling; pre-rift between 230 Ma and 160 Ma (1.2 °C/Myr) and syn-rift to present between 95 Ma and 0 Ma (0.6 °C/Myr). Ec10: thermal history outlines a protracted cooling history from 400 Ma to 0 Ma (0.25 °C/Myr). Ec20: thermal history displays protracted cooling from 400 Ma to 0 Ma (0.15 °C/Myr). Ec2: thermal history exhibiting

cooling from syn-rift to present between 66 Ma – 0 Ma (0.8 °C/Myr). Ec8: thermal history showing 2 significant cooling periods; pre-rift between 250 Ma and 190 Ma (1.3 °C/Myr) and syn-rift to present between 95 Ma – 0 Ma (0.7 °C/Myr). Ec22: thermal history showing two periods of cooling; pre-rift between 400 Ma and 160 Ma (0.3 °C/Myr) and syn-rift to present cooling from 90 Ma to 0 Ma (0.5 °C/Myr). Ec12: thermal history exhibiting protracted cooling from 20 Ma to 0 Ma (0.2 °C/Myr) followed by a post rift cooling episode to present (1 °C/Myr). Ec16: thermal history showing 2 periods of cooling; pre-rift between 360 Ma and 240 Ma (0.4 °C/Myr) and post-rift from 35 Ma to 0 Ma (0.7 °C/Myr).

(Figure. 6) Interpretation of the three cooling periods observed in thermal histories. (a) Conceptual model illustrating the rift flank uplift and erosion of the Cumberland Peninsula (line of section found in Fig. 1). Rift flank uplift of the SE margin instigates an erosional scarp retreat, while behind the escarpment fluvial systems, and later, glaciers erode valleys and fjords into the landscape, producing the modern geomorphology. (b) Flow accumulation analysis of the modern topography and bathymetry outlines two separate erosional systems, one converging at Quklavuk Island and another at Padloping Island. This would suggest the glacial systems have overprinted the Mesozoic fluvial systems and that the modern topography is simply a reflection of the ancient landscape. Offshore Cretaceous sands are found at the sea floor ~15 km NE of these onshore outcrops further supporting the concept of major Cretaceous fluvial systems (MacLean et al., 2014). (c) Paleo-geography of Laurentia suggests uplift of the Hudson Bay Basin in the Devonian and elevated Caledonides to the SE may have directed fluvial systems north over the Canadian shield, across the Cumberland Peninsula (red) and deposited in to the Sverdrup Basin, resulting in cooling from the Carboniferous to Triassic. Paleomap taken from Blakey & Wong (2003).

(Figure. 7) Results of 2D flexural model with Flex2D (Allmendinger et al., 2011) with initial model assumptions found in the text. Filling of the fjords, deemed as a simple estimation of the erosion, pushes down the lithosphere and gives the pre-erosion topography (grey),

which appears 90.7 m lower than the modern-day topography. These results suggest that differential unloading of the lithosphere does promote growth of the topography and that the topography of Cumberland Peninsula today is maintained by this isostatic response.

(Table. 1) Table of apatite (U-Th)/He data from the Cumberland Peninsula.

¹ Mean is the arithmetic mean age for each sample calculated from ages in black text. Those in grey text represent grain ages that have been excluded for being either <1 Ma or >1 Ga.

² $eU = [U] + 0.235[Th]$.

³ r' is the spherical equivalent radius.

⁴ F_t is the calculated correction factor from Farley et al. (1996).

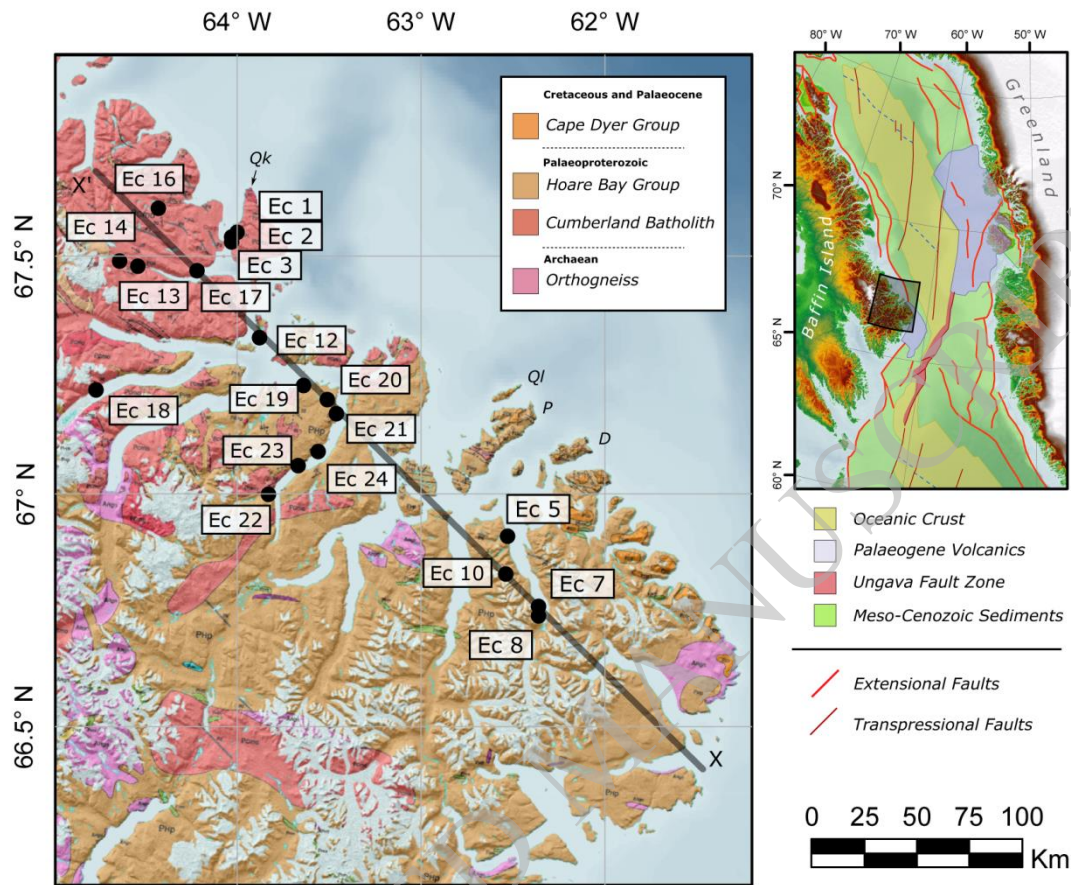
⁵ Corrected age is calculated from Measured Age / F_t .

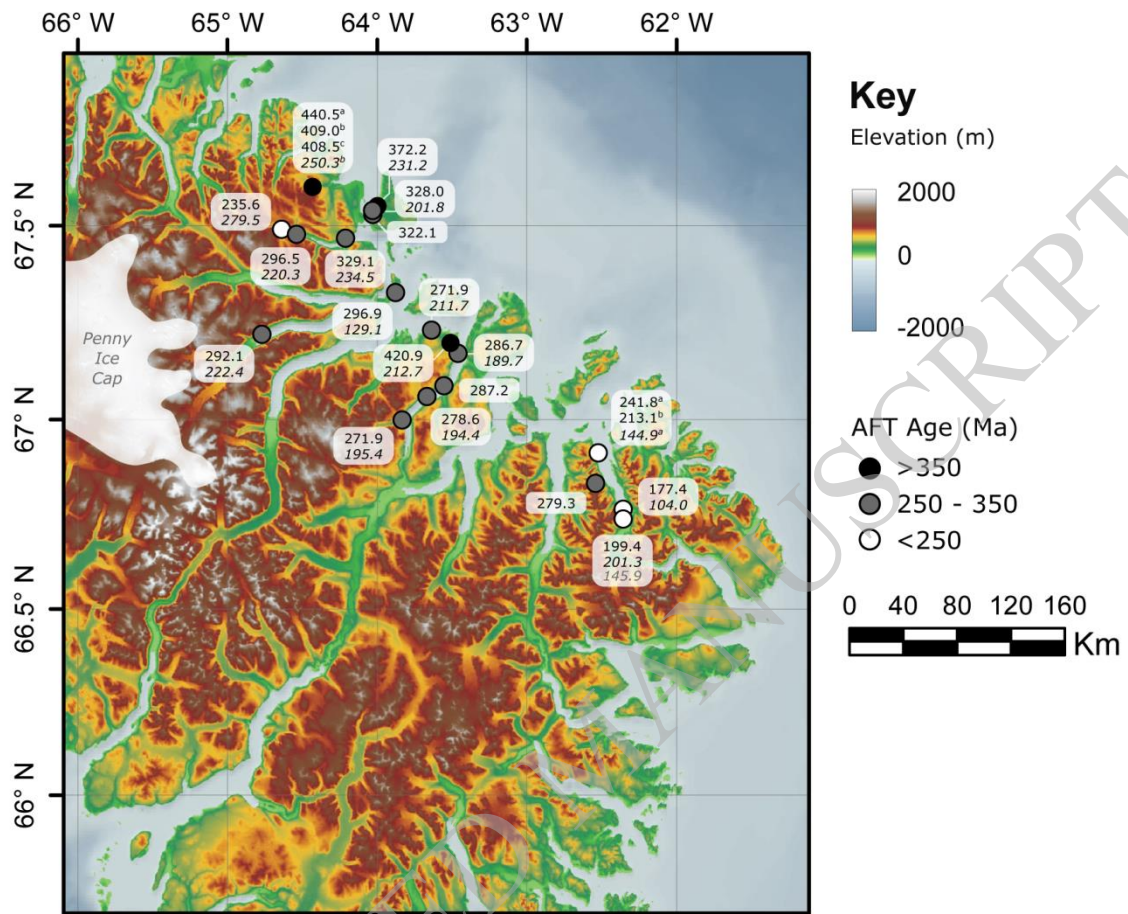
ACCEPTED MANUSCRIPT

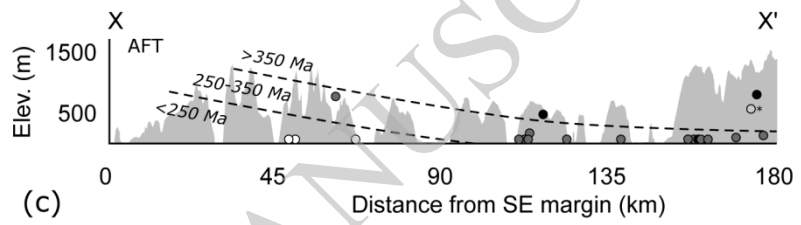
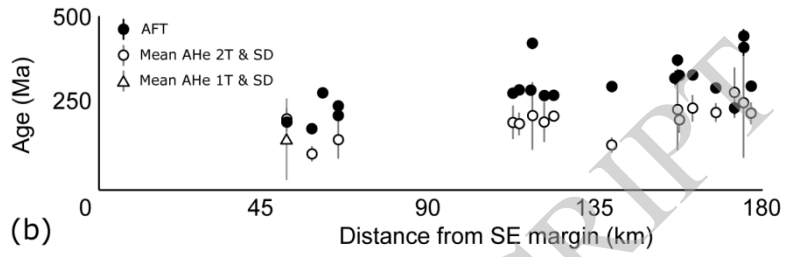
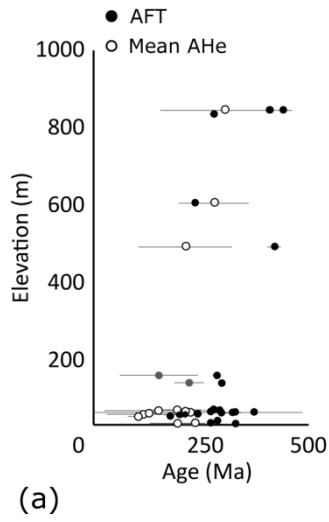
Sample (mean) ¹	He (ncc)	U (ppm)	Th (ppm)	Sm (ppm)	eU ² (ppm)	Length (μm)	Width (μm)	r ³ (μm)	Ft ⁴	Measured Age (Ma)	Corrected Age ⁵ (Ma)		
Ec1 (231.2)	a	0.00	14.71	25.80	41.68	20.77	152	102	57.3	0.7 4	0.10 ± 0.01	0.13 ± 0.01	
	b	0.13	11.1	5	3	37.08	5	174	75	46.3	8	5.51 ± 0.28	8.09 ± 0.40
	c	7	48.93	16.02	76.44	52.69	203	110	64.9	0.7 7	460.80 ± 23.04	597.86 ± 29.89	
	d	2.12	0.30	1.00	0.30	0.54	253	134	79.5	0.8 1	3790.3 ± 7	4666.6 ± 9	
	e	3.74	59.66	10.30	134	62.08	218	87	54.4	0.7 3	227.29 ± 11.36	312.49 ± 15.62	
EC2 (201.8)	a	8.75	87.58	23.09	976	94.00	156	88	51.6	0.6 1	267.41 ± 7.94	311.94 ± 9.23	
	b	3.08	59.70	4.92	1061	62.13	153	66	40.9	0.7 4	181.06 ± 6.58	220.17 ± 7.97	
	c	2.55	46.07	10.97	1219	50.13	174	93	54.9	0.7 3	153.64 ± 5.07	178.67 ± 5.88	
	d	2.92	44.71	12.40	800	48.59	144	85	49.0	0.6 0	204.29 ± 7.40	242.22 ± 8.76	
	e	3.36	79.83	4.69	1020	82.17	149	79	46.8	0.7 8	202.59 ± 6.67	242.87 ± 7.97	
Ec5a (144.9)	a	0.50	104	466	92.00	214	182	95	56.5	0.7 4	231.88 ± 3.18	323.75 ± 4.50	
	b	0.90	26.11	4.26	35.34	27.15	243	101	62.7	0.7 6	94.74 ± 0.91	124.09 ± 1.19	
	e	1.62	17.95	7.30	26.14	19.71	173	110	62.6	0.8 6	102.61 ± 0.95	136.42 ± 1.26	
	f	1.46	11320	1271	100	11619	376	117	75.9	0.7 0	0.17 ± 0.00	0.21 ± 0.00	
	h	4.49	41.18	8.70	46.00	43.27	360	132	83.1	0.8 2	150.23 ± 1.25	183.02 ± 1.51	
Ec7 (104.0)	a	1.09	26.72	3.86	64.05	27.71	184	100	59.0	0.7 5	112.16 ± 4.05	129.08 ± 4.65	
	b	0.24	17.82	2.98	54.61	18.59	132	78	45.3	0.6 7	86.79 ± 5.18	104.48 ± 6.23	
	c	1.46	30.77	4.55	69.82	31.92	138	89	50.6	0.7 1	142.50 ± 5.03	169.79 ± 5.98	
	d	0.33	21.01	2.87	46.32	21.74	127	83	46.8	0.6 8	97.57 ± 5.61	116.79 ± 6.71	
	e	0.28	18.06	4.10	46.11	19.08	149	77	45.9	0.6 8	81.14 ± 4.60	98.57 ± 5.58	
Ec8 (201.3)	b	-	0.29	0.29	0.55	0.35	241	118	71.1	0.7 9	- ± -	- ± -	
	d	4.66	22.38	4.65	53.00	23.54	228	135	78.1	0.8 1	235.37 ± 1.88	292.22 ± 2.32	
	f	3.22	28.79	10.47	101	31.37	195	157	84.0	0.8 2	206.00 ± 17.00	257.00 ± 22.00	
	g	0.47	9.50	3.54	44.77	10.39	193	136	75.4	0.7 0	146.53 ± 1.98	185.63 ± 2.50	
	i	1.56	13.59	6.90	53.00	15.27	138	120	62.7	0.6 6	217.14 ± 2.13	297.47 ± 2.91	
Ec81T (145.9)	a	0.64	13.12	4.46	40.20	14.22	197	151	240.4	0.9 4	74.82 ± 0.59	80.43 ± 0.64	
	b	0.33	13.06	5.41	46.72	14.39	124	137	194.9	0.9 2	92.27 ± 1.11	103.65 ± 1.25	
	c	0.51	9.14	4.57	46.62	10.27	173	130	207.8	0.9 3	127.44 ± 1.15	138.55 ± 1.25	
	d	11.0	92.40	82.65	1	6	180	165	249.7	0.9 4	164.58 ± 1.23	177.67 ± 1.33	
	e	0.70	7.48	4.62	39.92	8.62	189	135	219.3	0.9 3	156.59 ± 1.25	169.31 ± 1.35	
	f	0.55	10.89	2.77	33.77	11.58	174	124	201.0	0.9 3	124.59 ± 1.21	135.56 ± 1.31	
	h	0.50	12.63	4.33	78.07	13.74	175	138	218.2	0.9 3	79.67 ± 0.77	86.38 ± 0.84	
	i	0.79	11.98	4.22	53.45	13.03	239	145	245.3	0.9 4	105.27 ± 0.93	112.56 ± 1.00	
	j	0.27	9.18	5.53	50.13	10.55	169	119	193.6	0.9 2	62.61 ± 0.75	68.44 ± 0.82	
	k	0.31	18.26	5.25	33.38	19.53	132	97	156.1	0.9 0	113.52 ± 1.43	126.84 ± 1.60	
	l	0.66	23.60	5.37	79.80	24.96	178	118	195.0	0.9 2	112.37 ± 1.07	122.42 ± 1.17	
	m	0.21	11.68	5.45	49.51	13.02	129	109	168.7	0.9 1	66.65 ± 1.03	74.31 ± 1.15	
	n	0.24	14.02	4.28	59.09	15.10	113	115	168.0	0.9 1	91.91 ± 1.34	103.94 ± 1.51	
	o	0.35	9.10	6.19	53.46	10.62	103	139	182.0	0.9	131.76 ± 1.51	160.78 ± 1.84	

									7	2				
	p	2.92	38.62	5.39	70.18	39.97	176	122	199.2	0.92	197.95	± 1.56	215.20	± 1.69
	q	1.38	14.50	3.59	55.98	15.41	175	201	281.8	0.95	166.88	± 1.28	181.36	± 1.39
	r	1.02	84.35	13.68	71.00	87.65	134	99	159.8	0.91	90.51	± 0.79	100.85	± 0.88
	s	0.25	6.05	3.13	12.26	6.80	123	99	155.6	0.90	77.43	± 1.05	86.99	± 1.18
	t	1.85	24.48	3.47	69.66	25.38	127	76	128.5	0.88	610.17	± 6.18	690.08	± 6.94
	u	1.74	17.52	3.85	84.80	18.52	165	120	194.3	0.92	271.03	± 2.01	295.59	± 2.19
Ec12	a	3.51	56.00	30.66	812	64.00	214	105	63.2	0.76	101.63	± 0.87	133.65	± 1.14
(129.1)	b	1.71	10.45	19.77	586	15.80	182	106	61.6	0.76	155.37	± 1.38	209.08	± 1.85
	d	5.83	5.19	1.93	3.09	5.65	231	80	51.1	0.71	0.83	± 1.76	1.16	± 2.46
	e	5.14	17.97	59.00	440	32.27	203	113	66.3	0.78	130.31	± 1.03	172.28	± 1.37
Ec13	a	3.25	17.10	3.25	511	18.48	218	113	67.3	0.78	210.66	± 1.87	270.67	± 2.39
(220.3)	b	5.24	19.30	2.08	912	20.89	224	126	73.8	0.80	278.20	± 2.51	348.96	± 3.13
	c	2.65	29.85	1.56	989	31.41	186	103	60.5	0.75	187.63	± 1.74	248.91	± 2.29
	d	1.56	54.00	9.80	1433	58.00	137	76	44.6	0.67	202.17	± 2.04	301.51	± 3.01
	e	2.96	29.14	4.51	809	31.18	181	86	52.1	0.72	222.69	± 1.96	309.52	± 2.71
EC14	a	0.88	23.34	5.92	685	25.56	177	64	40.7	0.64	208.00	± 10.00	255.00	± 12.00
(279.5)	b	2.64	21.37	1.31	543	22.33	163	86	51.3	0.71	418.00	± 19.00	495.00	± 23.00
	c	2.56	22.38	4.10	667	24.15	191	108	63.1	0.76	238.88	± 8.87	272.00	± 10.00
	d	3.75	25.01	2.12	563	26.19	194	114	66.0	0.77	273.59	± 9.98	309.00	± 11.00
	e	1.80	27.77	2.46	587	29.05	161	76	46.0	0.68	258.82	± 9.68	309.00	± 12.00
Ec16	b	48.59	47.48	1.60	553	49.00	353	166	100.8	0.85	510.55	± 3.99	596.45	± 4.72
(250.3)	d	0.00	0.06	1.57	3.32	0.43	115	62	36.6	0.60	35.41	± 50.08	65.57	± 92.74
	g	2.21	18.52	0.61	264	18.98	189	76	47.5	0.69	290.60	± 2.83	415.81	± 4.00
	h	2.09	67.00	2.20	615	68.00	199	83	51.5	0.71	257.94	± 2.65	358.14	± 3.65
	b	1.93	48.70	3.65	429	50.08	158	102	57.8	0.74	157.08	± 1.23	213.31	± 1.66
EC17	a	1.40	13.81	7.31	653	16.31	169	103	59.3	0.75	194.85	± 8.37	222.79	± 9.57
(234.5)	b	1.21	20.69	0.85	749	21.80	186	99	58.4	0.75	182.65	± 6.97	211.08	± 8.03
	c	0.97	18.76	1.78	912	20.28	167	67	41.7	0.65	277.00	± 18.00	336.00	± 21.00
	d	6.96	25.48	1.67	746	26.77	136	64	38.7	0.62	256.19	± 8.22	2.86	± 0.09
	e	0.61	12.65	1.40	618	13.73	179	70	43.7	0.66	262.00	± 21.00	316.00	± 25.00
Ec18	c	0.00	0.98	4.15	8.77	1.95	119	100	52.8	0.72	0.62	± 3.41	0.00	± 0.00
(222.4)	e	0.00	31.04	30.06	2.17	38.11	180	140	75.6	0.80	0.52	± 0.20	0.65	± 0.25
	f	1.41	49.00	29.23	813	57.00	151	74	44.6	0.67	195.42	± 1.99	292.23	± 2.96
	g	-	1.80	1.57	6.81	2.16	197	83	51.4	0.71	0.39	± 0.14	-	± -
	i	14.65	21.30	14.73	415	25.27	272	200	109.7	0.86	249.32	± 2.09	292.82	± 2.44
Ec19	a	5.00	24.39	12.21	590	27.97	198	126	139.3	0.89	196.73	± 1.27	221.91	± 1.43
(211.7)	b	9.06	43.85	6.07	774	46.21	216	126	136.8	0.89	232.45	± 1.64	261.69	± 1.84
	c	9.83	23.25	11.65	720	26.85	289	169	98.3	0.85	214.61	± 6.00	259.21	± 7.23
	d	1.60	19.41	7.85	667	22.07	216	80	50.8	0.71	204.47	± 9.06	231.00	± 10.00
	e	8.21	46.56	9.80	968	50.03	230	128	75.1	0.80	210.32	± 5.92	237.28	± 6.67

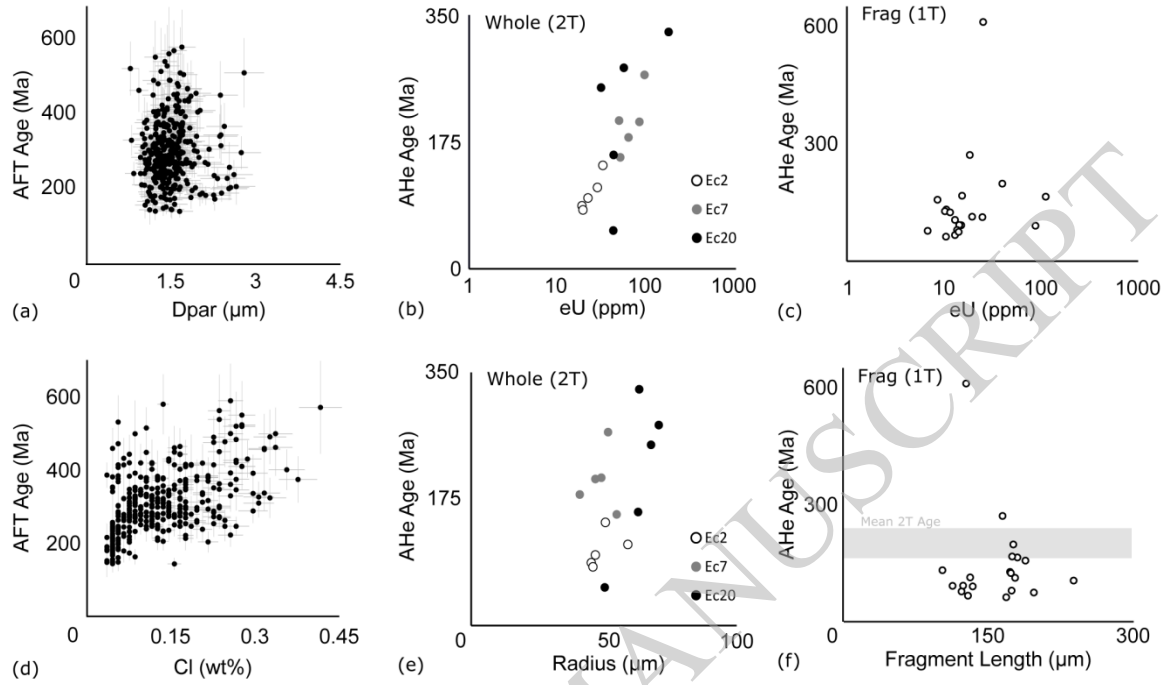
										0				
Ec20	16	6.48	48.00	30.92	181.0	55.00	211	121	70.7	0.7	277.18	± 2.42	353.49	± 3.07
(212.7)	27	1.04	39.23	10.92	26.9	41.79	137	89	50.4	0.7	52.71	± 0.54	75.88	± 0.78
	32	17.9	67.00	458	43.5	175	201	107	63.3	0.7	326.62	± 2.91	440.30	± 3.88
	43	8	29.72	3.21	32.1	30.47	237	112	67.8	0.7	249.90	± 2.43	319.23	± 3.08
	45	3.55	41.17	4.31	16.3	42.18	182	109	62.9	0.7	156.92	± 1.52	206.65	± 2.00
Ec21	a	2.52	25.60	0.16	405	26.13	327	137	85.0	0.8	141.41	± 1.08	171.35	± 1.31
(189.7)	b	10.2	22.82	1.97	460	23.84	510	179	114.	0.8	226.91	± 1.72	260.83	± 1.97
	c	23.8	19.37	8.64	8.9	21.41	266	129	78.0	0.8	0.30	± 5.70	0.40	± 7.10
	f	7	25.64	2.16	426	26.66	380	222	128.	0.8	179.31	± 1.37	203.67	± 1.56
	g	3.56	46.38	6.77	478	48.55	380	222	128.	0.8	211.11	± 1.70	239.77	± 1.93
Ec22	a	8.12	24.11	1.31	122	24.57	305	166	97.8	0.8	214.38	± 1.47	253.49	± 1.73
(195.4)	e	2.36	22.18	1.00	135	22.57	238	113	68.3	0.7	130.04	± 1.18	166.22	± 1.50
	f	4.69	28.40	2.21	143	29.09	263	168	95.5	0.8	163.32	± 1.28	194.95	± 1.52
	g	2.78	37.51	14.44	156	41.09	180	79	48.7	0.7	297.36	± 2.27	423.86	± 3.21
	h	4.05	40.55	15.73	85.6	44.35	183	146	78.3	0.8	172.05	± 1.19	217.91	± 1.50
Ec23	a	3.00	42.94	2.50	277	43.86	155	106	59.1	0.7	216.93	± 1.76	292.90	± 2.36
(194.4)	b	11.6	44.20	1.24	352	44.91	273	178	100.	0.8	261.91	± 1.86	309.35	± 2.19
	c	3	53.99	2.57	480	55.17	182	111	63.9	0.7	156.46	± 1.25	205.14	± 1.63
	d	2.51	0.94	1.09	0.41	1.19	145	99	55.3	0.7	-	± -	-	± -
	e	2.37	38.34	3.72	240	39.50	188	101	59.6	0.7	142.44	± 1.11	189.98	± 1.48



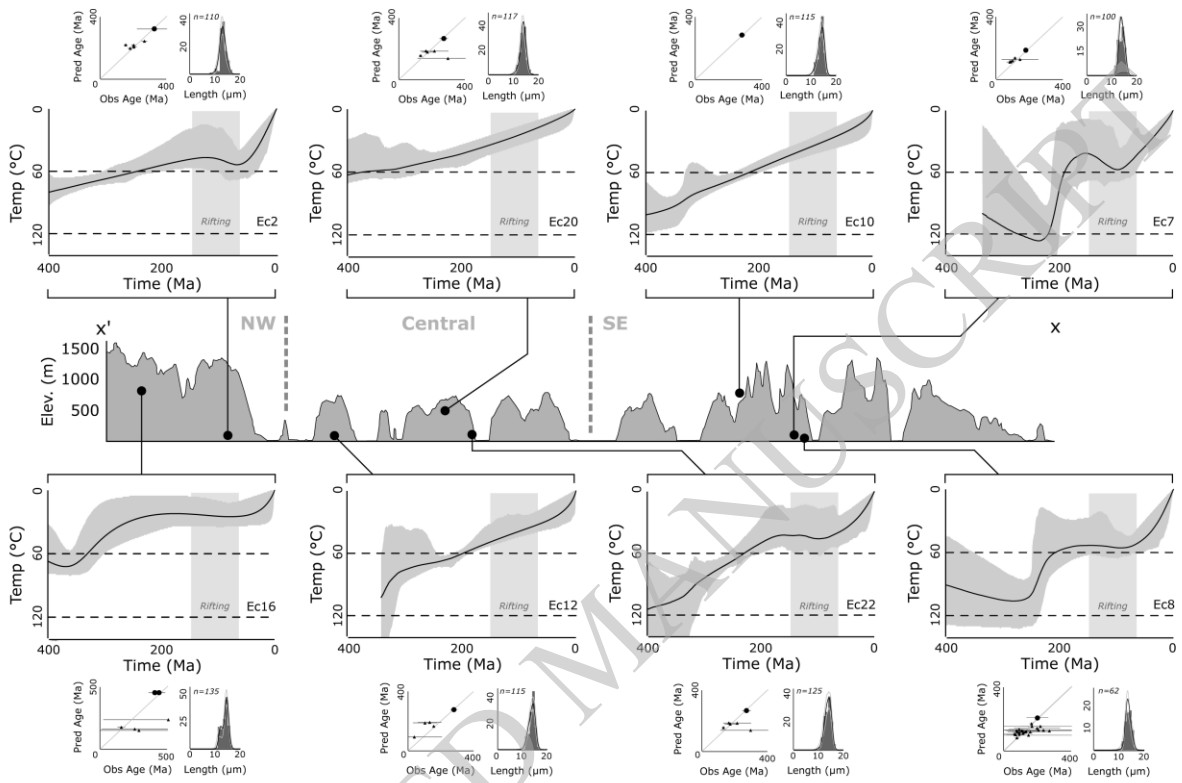




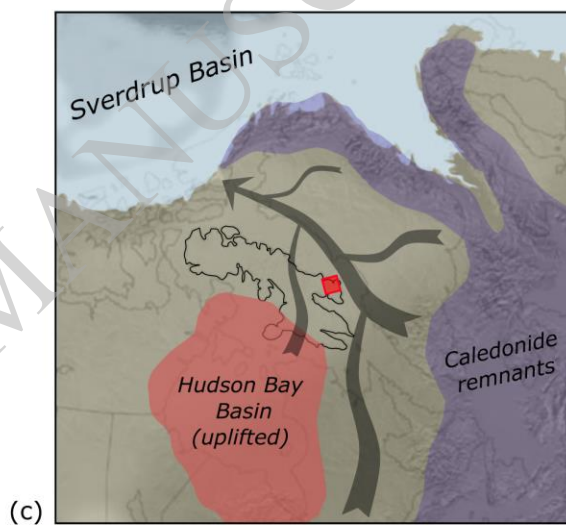
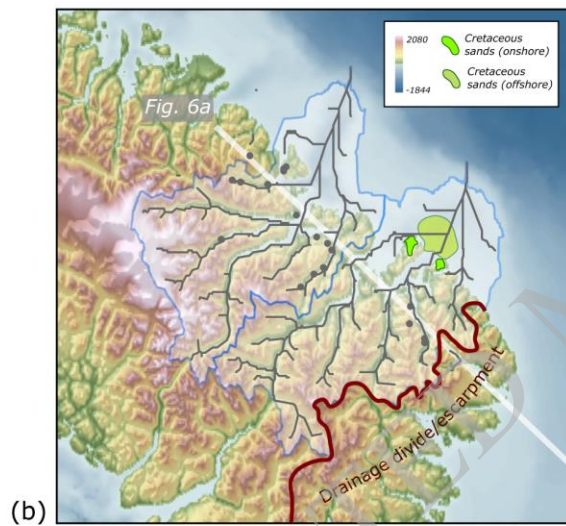
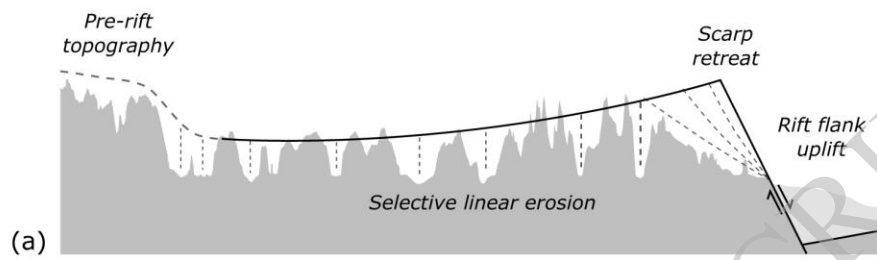
ACCEPTED MANUSCRIPT

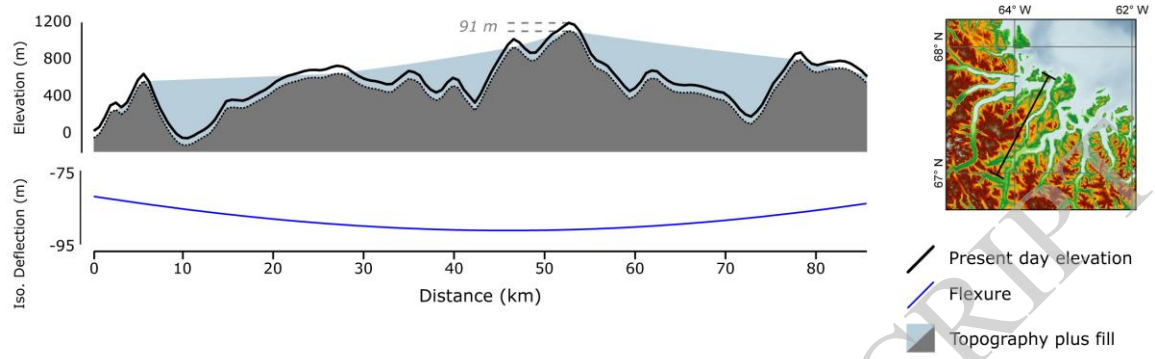


ACCEPTED MANUSCRIPT



ACCEPTED MANUSCRIPT





ACCEPTED MANUSCRIPT